Lowenergy ioninduced electron emission from gascovered surfaces

P. C. Smith, B. Hu, and D. N. Ruzic

Related Articles

Additional information on J. Vac. Sci. Technol. A

ADVERTISEMENT

Low-energy ion-induced electron emission from gas-covered surfaces

P. C. Smith, B. Hu,[a] and D. N. Ruzic
University of Illinois, Urbana, Illinois 61801

Measurements of ion-induced electron emission have been performed with helium and argon ions with energies between 300 and 900 eV on W, W with 10% Ti, Al, Al with 1% Cu, Al with 1% Si, Si, and Be. This article describes many of the important surface characteristics that influence the ion-induced electron emission. For low-energy ions, the substrate material was found to be less important as the velocity of the incident ion decreased. In the case of incident Ar^+ the substrate material had a negligible effect on the emission for this energy range. The presence of an adsorbed layer enhanced emission in all cases. Heating the substrates resulted in oxidation of the surfaces and a subsequent increase in emission. The electron emission from aluminum samples with smaller grain sizes was higher than samples of identical composition with larger grains. This effect is due to the greater number of adsorption sites resulting from the higher grain boundary area.

I. INTRODUCTION

The emission of electrons from a surface due to ion bombardment was first studied by Penning in 1928 under gas-discharge conditions.[1] Since that time the importance of these phenomena become clear along with the fact that a large number of variables are involved. A number of investigators have endeavored to determine the dependencies and have speculated as to their cause.[2-4] Among the more interesting variables studied are coverage of the surface, temperature of the surface, angular dependencies, work function of metal, and the charge of the incident ions.

Although the phenomena of ion-induced electron emission from surfaces have been observed since 1928, very little hard data are available for the case of low energy (<1000 eV) ions incident on real, gas covered surfaces due to experimental difficulties. Among these difficulties are the conditions of the sample and quality of the ion beam. The sample surface is affected by the gas coverage and the oxidation state. Both of these are affected by the temperature of the sample and the intensity of the ion beam. The creation of a low-energy ion beam of sufficient beam density and small energy spread is also problematical. Estimates of ion penetration depths utilizing the TRIM code vary from approximately 28 Å for Ar^+ to 100–125 Å for He^+. The ions then will certainly interact beyond the absorbed gas layer although charge exchange Auger processes (potential emission) will of course occur. The mean free paths for the emitted electrons are in the range of 5–20 Å in metals and semiconductors but can be many times higher in insulators. Therefore, the presence of these layers can be expected to significantly affect the probability of an electron's escape into the vacuum.[5] The apparatus described herein has been designed to measure the ion-induced electron emission coefficient of a material under low-energy ion bombardment. Among the features of this system are the selection of various ion species, energy ranges from several hundred eV down to a few eV, multiport target assembly allowing for the simultaneous measurement of several materials, inductive heating and liquid nitrogen cooling of the samples, residual gas analysis, computer controlled data acquisition, and fully bakable ultrahigh vacuum (UHV) pumping system capable of operation in the low 10^{-9} Torr range.

The apparatus was designed with the intention of studying the dependence of gas coverage on various substrates. The multiport target system of Fig. 1 allows the measurement of various substrates subject to identical background gas and thermal conditions. This work investigates the factors affecting the ion-induced emission including ion species and energy as well as substrate and adsorbed layer composition. In the sheath regions of plasmas the ion-induced electron yield is a critical parameter affecting sheath thickness and ion energy distribution and is therefore of interest for a wide variety of plasma-based phenomena including plasma based etching, sputtering magnetrons, and in studies of the diverter regions of magnetically confined fusion devices.[6-8] Early work with these phenomena quite naturally involved particle detectors since the measurement of an arriving ion current must allow for the departure of ion-induced secondaries. The energy range of 300–900 eV has been chosen as this represents most real applications and also because very little data are available for this regime.

II. EXPERIMENTAL APPARATUS

The ion beam is generated in a Colutron plasma based ion source.[9] The desired ion is produced from a stock gas fed to a manifold at 4 psig. The gas is emitted to the plasma chamber through a piezoelectric flow control valve. The gas is ionized in a small quartz chamber by electrons thermally emitted from a tungsten filament. Ions are extracted at 700–1000 eV from the resulting plasma. A significant advantage of this source is that the spread in energies is on the order of the thermal energy of the plasma (about 2 eV). At low anode voltages (e.g., ~50 V) metastable fractions can be as high as 2%. In these experiments however the source was operated at an anode voltage of 150–200 V where metastable fractions are negligible.[10]

A beam is created through a potential drop maintained between the ion gun and the primary lens. The primary lens is a three cylindrical element einzel lens. The first and third elements are maintained at ground potential while the center

---

[a]Current address: Intel Corporation, Beaverton, OR.
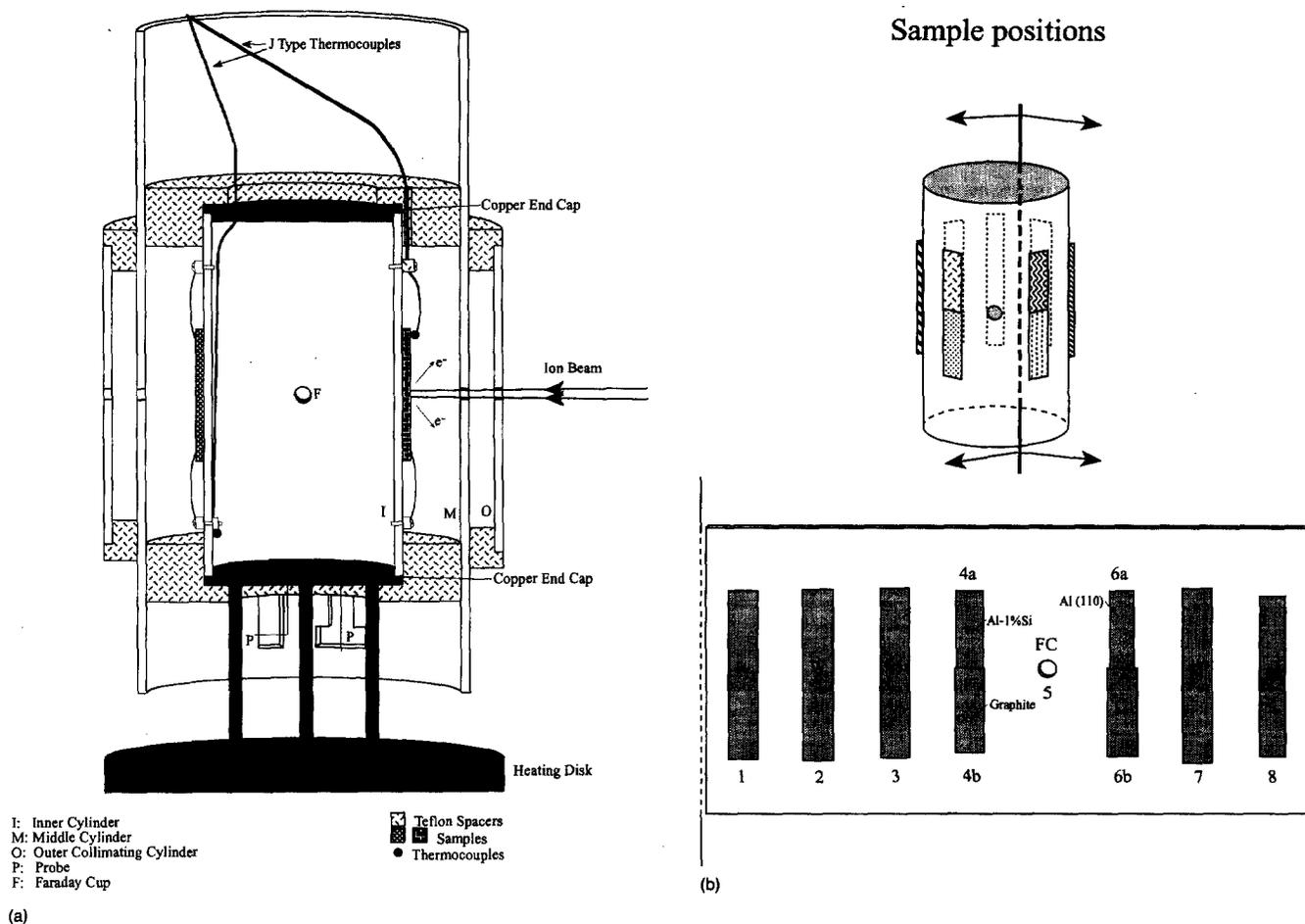
FIG. 1. (a) Cross section of the target assembly. (b) Schematic of typical sample layout.

element is biased to focus the beam into a column. The beam then passes between two horizontal electrostatic plates that serve to correct for any small variations in the vertical alignment of the system. After passing these plates the beam transits the $\mathbf{E} \times \mathbf{B}$ velocity filter where a specific charge to mass ratio is selected. Electrostatic plates steer the beam through a $5°$ bend, stripping neutrals from the beam path. The focused and species-selected beam passes next into the UHV chamber that has been baked to 185 °C. This chamber is initially isolated from the ion gun and is pumped with a turbo and cryopump to typically 2×10^{-9} Torr. When the UHV chamber is connected to the ion gun chamber, total pressure typically rises to 1×10^{-7} Torr. This pressure, of course, consists almost entirely of the noble stock gas with the partial pressures of all other species remaining at or below 2×10^{-9} Torr. The next element in the beam's path are two pairs of electrostatic raster plates placed vertically and horizontally. The voltage on these plates is varied by about 1.5 V (peak to peak) in a pattern similar to that in a cathode ray tube creating a uniform square pattern. This rastering ensures that any variations in intensity over the beam's cross section are averaged out over the grid pattern. Also, any translational variation on the order of the beam diameter (~ 0.2 mm) over the course of a reading is less likely to bring the beam into a

previously unexposed region of the target thus ensuring stable surface conditions.

The electrostatic repulsive force between the ions in the beam acts to spread the beam and decrease its intensity. The beam is transported at energies typically ≥ 700 eV so that the velocity of the ions is fairly high as they transit the system from source to target and the time of this interaction is minimized (5–16 μs). The deceleration of the beam to the desired energy and final focus is therefore performed as close to the target as possible. This is accomplished by a five element cylindrical electrostatic lens. The last element of this lens is floating at a potential that equals the extraction voltage minus the desired beam energy and is denoted as V_{35} since it is the potential of the third and fifth element in this five element lens.

The region surrounding the target assembly is completely bordered by a metal mesh screen that is maintained at the potential of the final element in the decelerator to ensure that the beam enters into a field free region. The beam transits this region and approaches the target assembly.

The target assembly consists principally of three stainless-steel coaxial cylinders (Fig. 1). Each of the cylinders is isolated from the others with Teflon spacers and the entire assembly is attached to an $XYZ\Theta$ manipulator. The potentials

on these cylinders are usually maintained equal to prevent defocusing of the beam although small biases can be applied (e.g., when verifying a negligible reflected ion fraction). In cases where the emission is on the order of 0.01 a potential of approximately 7 V is applied to the middle cylinder to prevent the escape of reflected neutral induced electrons. In cases where the emission coefficient is over 0.10 this is unnecessary as the neutral induced emission has a negligible effect. The outer cylinder serves to collimate the beam and, more importantly, by minimizing the signal from this cylinder, focus the beam. When properly focused the beam has a diameter on the order of 0.5 mm. The middle cylinder has holes that line up with those of the outer cylinder, but they are sized slightly larger to ensure that the incoming ion beam cannot strike it. Its purpose is to collect the electrons emitted by the samples. The samples are mounted on the inner cylinder. Two thermocouples monitor the temperature of the samples and the target assembly. The samples are held to the inner cylinder with copper beryllium sample clips with the exception of the upper portion of the tungsten sample which is held down by a thermocouple bead to monitor sample temperature. Positions 1, 2, 3, 7, and 8 are single sample locations and there are circular holes through the middle and outer cylinders radially outward from them. In contrast, positions 4 and 6 hold two samples each. Rather than a hole above them, these positions have a 2.5 mm wide slit which allows tracking the beam from one sample to the other by moving the manipulator up or down.

The samples measure approximately 1/4 in. × 3/4 in. × 0.06 in. They are ultrasonically cleaned in acetone and rinsed with methanol. This procedure is performed for all samples at least three times to ensure that the surface is free of contaminates. Adsorbed gas is sputtered away by the ion beam prior to recording yield values. Doses of approximately 1.5×10^{16} cm^{-2} were necessary for stable readings in close agreement with the data of Baragiola et al.[11] in spite of the lower energies used here.

III. DATA REDUCTION

The ion-induced electron emission coefficient γ is defined as the ratio of electrons emitted (I_e) to ions incident (I_i) therefore

$$\gamma = \frac{I_e}{I_i}. \tag{1}$$

The current on the inner cylinder (I) is due both to the arrival of ions and the departure of electrons

$$I = I_e + I_i. \tag{2}$$

There will necessarily be a small fraction of electrons lost through the aperture in the middle cylinder. The actual electron current is then slightly more than that collected on the middle cylinder (M). This discrepancy can be accounted for by calculating the fraction of electrons that are lost through this aperture and evaluating a geometric correction factor (g) to modify the current recorded to reflect the actual electron current. The electron current then can be represented by

$$I_e = gM. \tag{3}$$
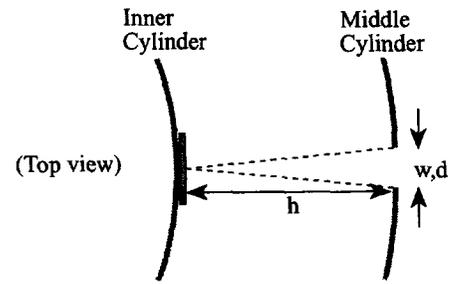
h: height above surface to middle cylinder
w: width of slit aperture
d: diameter of round aperture

FIG. 2. Top view section of target assembly.

Combining Eqs. (1), (2), and (3)

$$\gamma = \frac{gM}{I - gM}. \tag{4}$$

The calculation of the geometric correction factor is based on the solid angle represented by the aperture above the sample. The shape of the aperture in the middle cylinder is either round (positions 1, 2, 3, 7, 8) or rectangular (positions 4 and 6).

For the round aperture (Fig. 2) in terms of the diameter of the aperture (d) and the distance from the middle cylinder to the sample surface (h) the geometric correction factor is

$$g = \frac{h^2 + \left(\frac{d}{2}\right)^2}{h^2}. \tag{5}$$

The geometry of the slit aperture is more involved but the resulting integrals are evaluated numerically. In both cases a cosine distribution of the emitted electrons has been assumed.

The sources of error involve the geometric correction factor g and the currents on the inner and middle cylinders denoted by I and M, respectively. These terms include machining errors (Δg), zeroing error (ΔI_{zero}), reading error ($\Delta I_{reading}$), signal variation ($I\Delta_{var}$), inherent meter error (ΔI_{meter}), zeroing error (ΔM_{zero}), reading error ($\Delta M_{reading}$), and inherent meter error (ΔM_{meter}). Of these errors all are completely independent with the exception of ΔI_{meter} and ΔM_{meter}. The inherent meter error for the Keithley 416 Picoammeter is 2% of full scale. This error however will affect both the inner and middle current readings in the same manner and are therefore correlated effects. Specifically they are related as

$$\frac{\Delta I_{meter}}{I_{fs}} = -\frac{\Delta M_{meter}}{M_{fs}} = \alpha, \tag{6}$$

where I_{fs} and M_{fs} are the full scale values and α is the inherent meter deviation. The minus signal on the right-hand side is due to the opposite polarity of the inner and middle
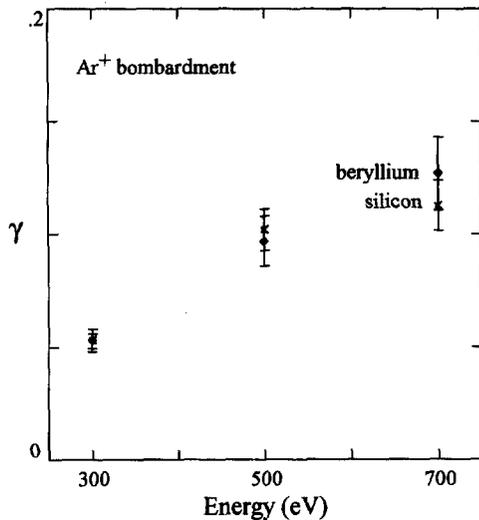
FIG. 3. Ion-induced electron emission coefficient from incident Ar^+ as a function of energy for Be and Si substrates.
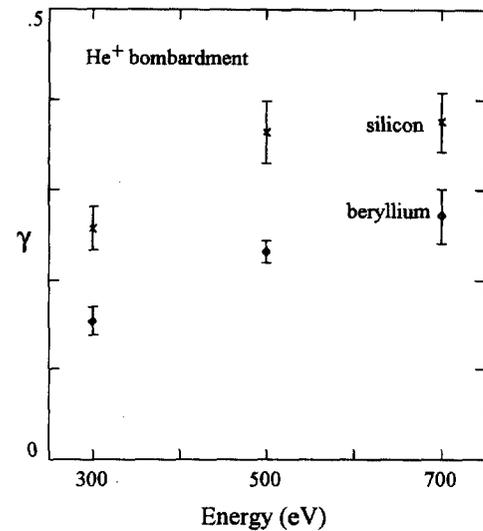
FIG. 4. Ion-induced electron emission coefficient from incident He^+ as a function of energy for Be and Si substrates.

currents. Since the meter specification is $\pm 2\%$, $-0.02 \leq \alpha \leq 0.02$. Although ΔI_{meter} and ΔM_{meter} are related, the meter error itself is independent of the other errors so that correlation of Eq. (6) is used to relate ΔI_{meter} and ΔM_{meter}

into a single meter error that is independent of the other sources of error and to use this expression as a term in an expression for the total error.

The equation for the error is then

$$\Delta \gamma(M,I,g) = \sqrt{\left(\frac{\partial \gamma}{\partial I}\right)^2 (\Delta I)^2 + \left(\frac{\partial \gamma}{\partial M}\right)^2 (\Delta M)^2 + \left(\frac{\partial \gamma}{\partial g}\right)^2 (\Delta g)^2 + \left(\frac{\partial \gamma}{\partial I} \cdot I_{fs} - \frac{\partial \gamma}{\partial M} \cdot M_{fs}\right)^2 (\alpha)^2}. \tag{9}$$

The values for the ion-induced electron yield that are presented in this paper are calculated from data runs consisting of several data points each calculated by the above procedure. A typical run involves as many as 60 of these data points and may take as long as 90 min. The first few points of a run represent a transient response as the adsorbed layer attains an equilibrium between the ion-induced desorption, thermal desorption, and adsorption from the background. The points following this transient are fitted with a least-squares fit line weighted by the reciprocal of the square of the error.

IV. RESULTS AND DISCUSSION

Figures 3 and 4 compare γ from Si and Be under Ar^+ (Fig. 3) and He^+ (Fig. 4) bombardment at 300, 500, and 700 eV. Second, surface coverage effects are dependent upon the incident ion flux and it is important that a comparable flux be delivered to the substrates of all of the energies. Although measurable signals can be obtained at energies below 300 eV, the effects of space charge markedly reduce the ion flux. Comparisons made to higher energies cannot discriminate between an effect due to ion kinetic energy and one due to surface coverage resulting from the flux difference. The phenomena of ion-induced electron emission can be broadly

classified by the source of energy for the process. When the ionization energy of the incident ion is the source, the process is termed potential emission, and when the energy taken from the kinetic energy of the ion it is termed kinetic emission.[12] Potential emission is nearly independent of the incoming ion's kinetic energy since the emitted electron's energy is derived from the ion's ionization energy. However kinetic emission due to noble gas ions is expected to scale roughly linearly with the kinetic energy of the ion.[13] The electron yields of Figs. 3 and 4 show the expected increase with ion kinetic energy consistent with the work of other researchers (e.g., Alonso et al.[14]).

Figures 3 and 4 show that in all cases the electron emission from helium ions was higher than for argon ions. There are two principle differences between the incident helium and argon ions. First, the ionization energy of helium is 24.6 eV whereas for argon it is 15.8 eV. This suggests that the potentially emitted electrons resulting from incident helium ions will have a higher energy and thus a higher probability of escaping the surface. Since kinetic emission will not be affected by the ionization energy, this effect should be greatest at the lower energies where the majority of the electrons emitted are due to potential emission. This trend is clearly evident by comparing the ratio of electron yields of He^+ vs

Ar^+. The ratio is largest for the lower energies where potential emission is dominant.

A difference in ionization energy alone is not sufficient to explain the higher yield from the helium atoms. The higher energy data where kinetic emission is important still shows the helium atoms emitting more electrons. Also, the difference of 8.8 eV in ionization energies is not large enough to explain the two- to fourfold ratio between the yields. The second major difference between the incident ions is that for a given energy, the mass difference results in very different ion speeds. A ratio of 3.2 for the speeds when compared to the data in Fig. 3 supports the conclusion that the yield scales with the speed of the incoming ion. The data for the semi-conductor silicon suggest a somewhat lower than expected increase in electron yield with speed.

Another notable feature of the data in Fig. 3 is that for incident argon ions there is very little dependence on the substrate material. To understand this effect it is important to recall the state of the surface being studied. Both the silicon and beryllium surfaces retain thin oxide layers covered with a small adsorbed gas layer. The electron emission from these surfaces then will be due to interactions with the gas layer and the underlying oxide layer to varying degrees. The chance that an ion will interact with the adsorbed gas layer will be roughly proportional to the time spent transiting that layer. This transit time in turn is proportional to the speed of the incoming ion. Although this layer is thin an electron liberated in this layer has a much higher probability of escape due both to its proximity to the vacuum and due to its large mean free path in the insulating adsorbed layer. For the same energy, the argon ions are 3.2 times slower than the helium ions, and will therefore be far more likely to interact with this adsorbed layer. Since the adsorbed layers of the beryllium and silicon samples were nearly identical, the electron emission due to the argon ions is nearly the same for both substrates. The helium ions in contrast interact with the substrate more readily. Figure 4 suggests that more electrons are emitted from a silicon substrate than a beryllium. This may be due in part to an increased role of the oxide layer on the surface of the silicon sample.

In addition to the studies on the silicon and beryllium systems, a number of measurements were performed on various sputtering targets provided by TOSOH SMD Inc. shown in Fig. 5. Although there are not enough points to evaluate the scaling accurately, it is interesting to note that the yield scales linearly to sublinearly with ion energy.

The adsorbed gas coverage has a pronounced effect on the electric emission. Specifically, as the layer thickness increases, the expected electron emission coefficient increases. Even though the amount of electrons liberated in this gas layer may be small, the electron has a much higher probability of emission since its mean free path length in the insulating gas layer is much larger than comparable electrons in the substrate. In order to explore these effects readings were taken at 19 and at 74 °C for the various materials in Table I.

In all cases the yield increased with temperature. This was directly counter to the expected result since it had been assumed that an elevated temperature would lead to a thinner adsorbed layer and subsequently less emission. The explana-
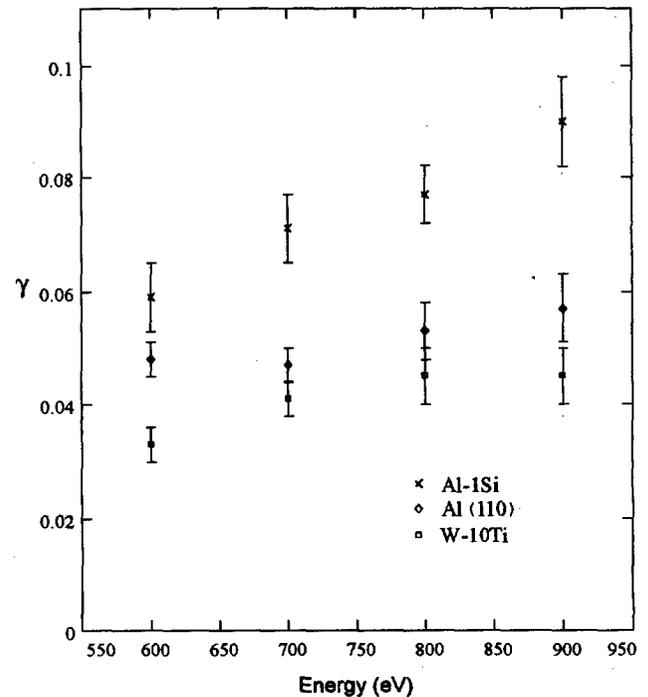
FIG. 5. Ion-induced electron emission coefficient from incident He^+ as a function of energy for Al–1% Si, Al(110), and W–10% Ti substrates.

tion was found in a close analysis of the residual gas analyzer data (Fig. 6). At 74 °C the hydrogen peak is elevated (this is a log plot). This suggests that water present in the background has dissociated on the surface of the substrate and formed either oxides or a chemisorbed adsorbate layer. Table I has been arranged in order of decreasing *percentage* change in the electron emission coefficient to illustrate that materials that readily form oxides are those most affected by the temperature increase. The formation of an oxide layer functions in the same manner as a thick adsorbed layer in that the emitted electrons produced have a high probability of emission due to the increased mean free path. This is due to the decreased electron scattering in an insulating layer as compared to the bulk metal or semiconductor.[5]

In reviewing earlier data, this effect was clearly observed. After the data presented in Table I were obtained, the filament on the ion source was replaced. Despite careful degas-

TABLE I. Effect of elevating substrate temperature (700 eV He^+).

	Substrate	19 °C	74 °C
Strong	Al–1%Si	0.37±0.02	0.46±0.04
oxide formers	Si	0.32±0.04	0.37±0.03
	Al–1% Cu(S)	0.39±0.03	0.48±0.06
	Al–1% Cu(M)	0.25±0.02	0.36±0.06
	Al–1% Cu(L)	0.18±0.01	0.23±0.02
Less strong	W	0.31±0.04	0.33±0.05
oxide formers	Be	0.24±0.01	0.25±0.02

TABLE II. Oxide effect in yield due to incident 700 eV Ar^+.

Substrate	Before	After	% change
Al(100)	0.047 ± 0.003	0.129 ± 0.010	174.5
Al–1% Si	0.071 ± 0.006	0.142 ± 0.013	100.0
W–10% Ti	0.041 ± 0.003	0.035 ± 0.002	−14.6

FIG. 6. Residual gas analyzer scans for the data in Table I. Partial pressures are in Torr.

sing of the filament and pumping of the gun chamber this maintenance unavoidably introduces some water to the gun chamber and subsequently a small amount is carried over to the main chamber. Table II shows the effect on the electron yield on the same target materials at identical temperatures immediately before and after the filament replacement. These reading show an increase in water vapor in the background gas. Aluminum is a strong oxide former and therefore sees a significant increase in emission. The three Al–1% Cu samples in Table I are identical in composition but differ in grain structure. The three samples are of medium (M), small (S), and large (L) grain size, respectively. Smaller grain sizes result in higher electron yields. This is a result of the larger density of grain boundaries on the surface of the sample with smaller grains. Oxide and adsorbates are more prevalent in the grain boundaries and the presence of insulating components such as these enhances electron emission. These aluminum samples were manufactured using a sintering and pressing process that resulted in significant porosity of the samples. The resultant grain boundaries are three dimensional and their effect on the surface is therefore accentuated. Once the background partial pressure of water vapor fell to its prevacuum break condition (about a week), γ returned to the previous value following any significant ion flux. In contrast the tungsten-titanium (W–10% Ti) samples exhibited a decrease in emission. This peculiar system is examined in more detail in a paper by Hendricks[15] where the ion-induced electron emission of W–10% Ti samples of varying porosity are found to have emission yields that vary by as much as 50%.

In the course of these investigations, it was found that the observed ion-induced electron emission yield (γ) varied significantly for different ion flux levels. To understand this variation, the adsorbed gas layer must be more closely examined. The steady-state adsorbed gas layer is the result of background gas adsorption, thermal desorption, and ion-induced desorption.

In any surface-gas system the resulting gas layer is the result of a balance between the adsorption of atoms from the background gas and the thermal desorption of the adsorbed atoms from the surface. When an ion beam is incident on the surface, elastic collisions with adsorbed gas atoms may transfer sufficient energy to those atoms where some of them are desorbed. There are three regimes to consider in this case. The first is where the ion flux is small enough such that ion-induced desorption may be neglected. In the other extreme, the ion flux is so large that the gas layer is quickly and nearly completely removed. In many practical applications however, the balance of all three desorption/adsorption mechanisms must be considered. In this experiment, conditions were established to create an equivalent ratio of fluxes
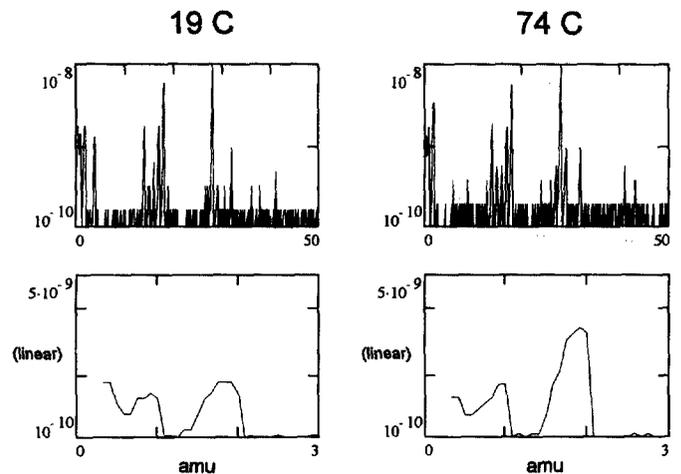
in order to investigate these phenomena. In general the experiments were conducted with an approximately 30 nA beam confined to a spot of approximately 1 mm in diameter. This resulted in an ion flux of 2.4×10^{13} $cm^{-2} s^{-1}$. When the valve connecting the gun and target chambers is open, the pressure at the target is about 10^{-7} Torr. This pressure corresponds to a flux of 3.8×10^{13} $cm^{-2} s^{-1}$ from the background gas atoms.

A series of experiments was performed to investigate these effects. The bulk of the studies utilized a common sputtering target of aluminum alloyed with 1% copper. This substrate was chosen primarily due to interest in this material as a sputtering target. Data from earlier measurements on graphite were also analyzed and revealed flux induced gas coverage effects as well. It is important to note at this point that the "high" flux levels referred to in this section are usually on the order of 30–40 nA. The electron emission yield data presented in the previous sections were performed at flux levels five times those levels and time was allowed for ion-induced desorption so that the effects of physisorbed gas layers on those readings can be considered small.

The experiments consisted of stepping the flux from low to high to low, or conversely beginning at a high flux stepping to low and back to high over the course of an hour. For the purpose of discussion the portion of the ion-induced electron yield plot corresponding to the initial flux level shall be denoted as region I and subsequent regions as II and III.

Figures 7(a) and 7(b) show the case where the flux was initially low (6–10 nA), then after about 20 min it was raised to its high level (30–40 nA) where it remained for an additional 20 min. The flux was then reduced to its low value for a final 20 min. In Fig. 7(a) the ion-induced electron yield begins very high at about 0.69. A high value for the initial reading is expected as the adsorbed gas layer is thickest at this point. As was previously discussed, the presence of a nonconducting layer increases the electron mean free path and subsequently increases the likelihood of emission. Over region I, γ decreases slowly as the ions desorb atoms in the gas layer. The substrate in Fig. 7(a) is at room temperature so
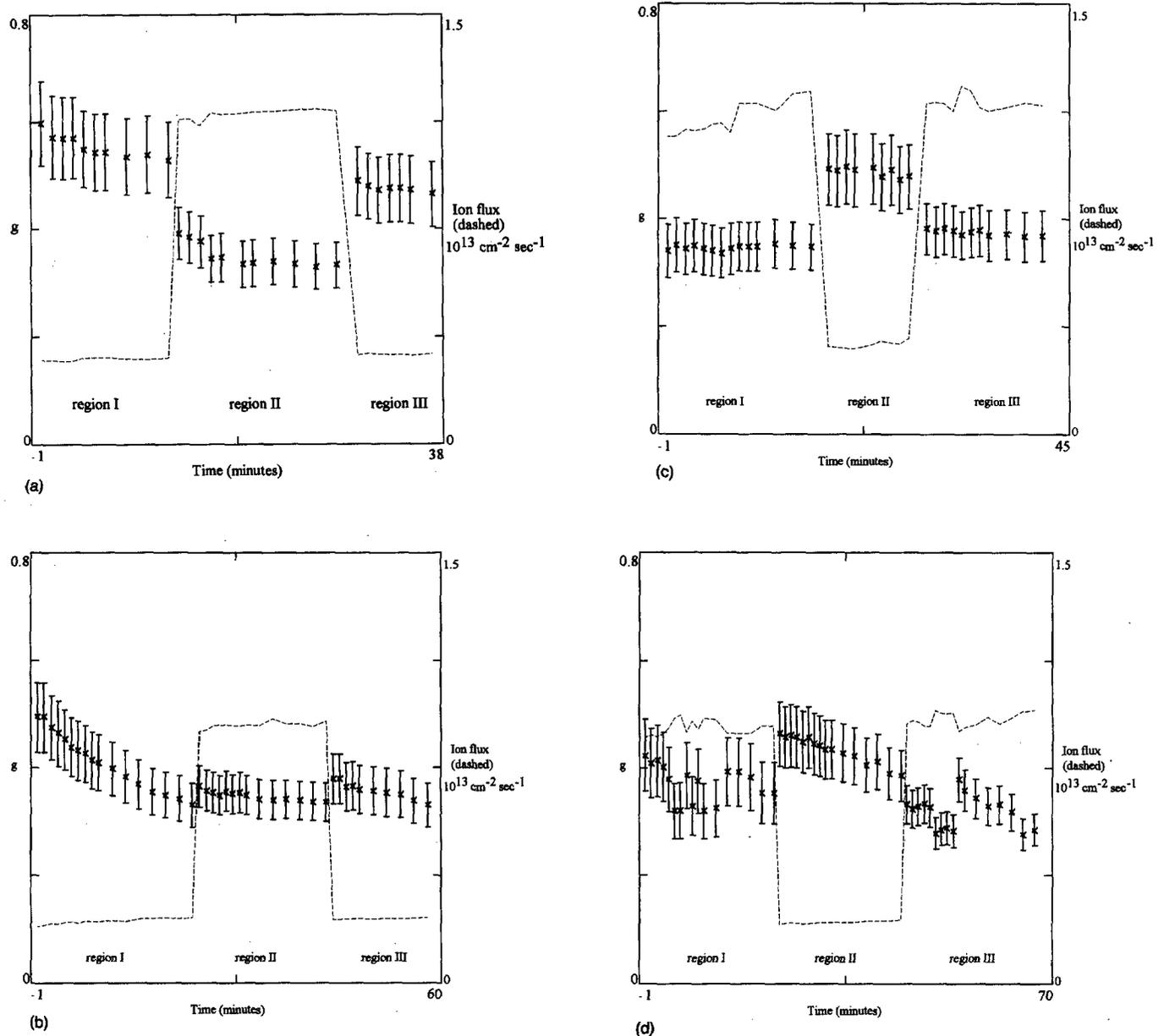
FIG. 7. The effect of flux on the emission coefficient. The 700 eV He$^+$ ion beam was rastered over the Al–1% Cu targets. Ion flux is shown on the right-hand scale. (a) The flux was increased then decreased at room temperature, 19 °C. (b) The flux was increased then decreased at an elevated temperature of 74 °C. (c) The flux was decreased then increased at room temperature, 19 °C. (d) The flux was decreased, then increased at elevated temperature, 84 °C.

that the initial gas layer is substantial as indicated by this slow decrease in γ. As the flux is increased the adsorbed layer is rapidly desorbed and subsequently γ decreases. After a rapid drop over the first few minutes an apparent steady state is reached at approximately 19 min corresponding to a nearly gas free surface. At the beginning of region III the flux is again lowered. The gas layer grows and approaches an equilibrium value that corresponds to the equilibrium gas layer reached by the balance of the adsorption/desorption mechanisms. Figure 7(b) shows results from an identical experiment conducted at 74 °C rather than 19 °C. The decrease in region I of γ is far more pronounced due to the fact that the adsorbed layer is much thinner and the ion-induced desorption can remove it more quickly. The initial value of γ is also lower. The transitions from regions I to II and II to III

both show a slight increase in γ. This is due to shifting the beam as the transport conditions are changed. Part of the beam intercepts a portion of the target that has not been desorbed. In all three regions the layer is thin enough so that an equilibrium γ is reached.

Figures 7(c) and 7(d) show the case where the flux began at the high flux level, reduced to the low flux level, and then returned to the high flux level. Each of these levels were maintained for approximately 20 min. Figure 7(c) shows the room-temperature case. The initial high flux is sufficient to rapidly achieve a γ corresponding to very little gas coverage. As the flux was lowered at the transition to region II the gas layer increased and subsequently γ increased. As the flux was again raised, γ returned to near the value of region I. Figure 7(d) shows a data run at 84 °C. The characteristics are

similar to those of Fig. 7(c) with the exception that this run was more sensitive to slight variations in the ion beam transport parameters. The transition to region II indicates a rapid increase in γ followed by a slow decrease. This is a result of the initial slight translation of the beam into an area of higher gas coverage due to the change in intensity and the subsequent slow desorption of this gas layer (slow as a result of the low flux level). The gas layer in this region is thicker and therefore the γ increases.

The effects of sample preparation techniques were investigated for the cases of silicon and tungsten. An RCA cleaned silicon sample stored in inert gas was compared to another sample stored in air and ultrasonically cleaned and prepared as described above. The resultant measurements of emission from these surfaces were the same and correspond to those reported above. Similarly tungsten samples were examined with and without a residual water vapor adsorbed layer and the resulting steady-state emission yields were the same. Although the transient behavior of these samples varied with the preparation methods, the ultimate steady-state values are reproducible.

The effect of the reflected flux on the recorded values of emission needs to be considered. This reflected flux can affect the readings in two ways. First and most importantly the reflected particles are able to strike the middle (emitted electron) collection cylinder of Fig. 1 and result in kinetic emission of electrons which leave this cylinder and strike the inner cylinder. This effect acts to depress the apparent emission. This effect is only important in cases where the reflection coefficient is greater than about 0.2. Ar^+ being a heavy ion has a very low reflection coefficient and there is no perceptible effect. He^+ in contrast, when striking a heavy target can result in high reflection fluxes and further experiments have indicated that this effect can depress the apparent emission by as much as 40%. The second effect is the influence of the fraction of this reflected flux that is ionized. In most cases, this fraction is very small and can be ignored. However, as shown by Chen and Rabalais,[16] an oxide layer can increase this fraction by as much as 10 times. Therefore, in cases where the surface is known to consist of a significant thick oxide layer, this effect should be evaluated. The present experimental apparatus does not allow for the measurement of the effect of reflected ions however in those cases where an oxide layer is present, calculations indicate that the emission value may be up to 25% higher than reported.

V. SUMMARY AND CONCLUSION

The experiments on the silicon and beryllium substrates indicated a number of characteristics of the ion-induced electron yield. In particular as the energy is increased, γ increases linearly in systems where the adsorbed layer is less important. As the adsorbed layer thickness increases this relationship becomes less than linear and γ begins to scale with the velocity. This was also observed in the study of various sputtering targets of Fig. 5. The behavior of nonmetals in particular seems to deviate from the expected linear behavior. "Expected" in this context refers to the theories of ion-induced electron emission.[17-19] These theories typically assume flat, gas-free metals.

For incident helium atoms, γ was found to be greater than that for the argon ions. This is due, in part, to the higher ionization energy of the helium ions, but is due primarily to their higher velocity for a given energy.

The importance of the substrate is diminished by the presence of an adsorbed layer. The thicker this layer, the higher the probability that the electron liberation event will occur in the adsorbed layer rather than in the substrate. For a given adsorbed layer, the speed of the ion will determine the transit time. A slower ion is more likely to interact with the adsorbate than the substrate. This effect was clearly demonstrated in the study of argon and helium on beryllium and silicon where the slow (for a fixed energy) argon ions resulted in similar γ's, regardless of the substrate.

Studies on the influence of temperature showed that the predominant effect was the chemisorption and oxidation on the surface of the sample leading to an increase in γ for materials studied.

For aluminum alloys with varying grain sizes, the smaller grain sizes resulted in higher γ. This is due to the increased surface grain boundary area and subsequent adsorption on these sites.

The effect of the incident ion flux needs to be considered when its magnitude is on the order of the background gas flux to the surface. The presence of ion-induced desorption results in a reduction of the γ as a consequence of the thinner adsorbed layer. Depending on the flux levels a steady state is eventually reached where there is a stable adsorbed layer thickness. If the ion current is high enough, this layer will be negligibly small. As beam parameters are changed the beam may become translated to a small amount such that part of the beam falls on an area with a thicker gas layer. This will result in a momentary increase in the γ until this layer is desorbed by the beam.

ACKNOWLEDGMENTS

[1]F. M. Penning, Physica 8, 13 (1928).
[2]W. O. Hofer, Scanning Microsc. Suppl. 4, 265 (1990).
[3]B. A. Brusilovsky, Appl. Phys. A 50, 111 (1990).
[4]G. M. McCracken, Rep. Progr. Phys. 38, 241 (1975).
[5]D. Hasselkamp, Particle Induced Electron Emission II, Springer Tracts in Modern Physics Vol. 123, edited by G. Höhler (Springer, Berlin, 1992).
[6]Z. Ropcke, Contrib. Plasma Phys. 26, 67 (1988).
[7]J. Mandrekas, C. E. Singer, and D. N. Ruzic, J. Vac. Sci. Technol. A 5, 2315 (1987).
[8]W. D. Westwood, Handbook of Processing Technology (Noyes, Park Ridge, NJ, 1990).
[9]M. Menzinger and L. Wahlin, Rev. Sci. Instrum. 40, 102.
[10]W. Hofer, W. Vanek, P. Varga, and H. Winter, Rev. Sci. Instrum. 54, 150 (1983).
[11]R. A. Baragiola, E. V. Alonso, J. Ferron, and A. Oliva-Florio, Surf. Sci. 90, 240 (1979).
[12]H. D. Hagstrum, Phys. Rev. 96, 336 (1954).
[13]O. B. Firsov, Sov. Phys. JETP 7, 308 (1958).

[14]E. V. Alonso, R. A. Baragiola, J. Ferron, M. M. Jakas, and A. Oliva-Florio, Phys. Rev. B **22**, 80 (1980).

[15]M. B. Hendricks, P. C. Smith, D. N. Ruzic, A. Leybovich, and J. E. Poole, J. Vac. Sci. Technol. A **12**, 1408 (1994).

[16]J. N. Chen and J. W. Rabalais, J. Am. Chem. Soc. **100**, 46 (1988).

[17]E. J. Sternglass, Phys. Rev. **108**, 1 (1957).

[18]M. Rösler and W. Brauer, Phys. Status Solidi B **K85**, 156 (1989).

[19]J. Devooght, J. C. Dehaes, A. Dubus, M. Cailler, and J. P. Ganachaud, *Particle Induced Electron Emission I,* Springer Tracts in Modern Physics Vol. 122, edited by G. Höhler (Springer, Berlin, 1991),